Angular velocity distribution of a granular planar rotator in a thermalized bath

J. Piasecki,[1] J. Talbot,[2] and P. Viot[3]
[1]*Institute of Theoretical Physics, University of Warsaw, Hoża 69, 00 681 Warsaw, Poland*
[2]*Department of Chemistry and Biochemistry, Duquesne University, Pittsburgh, Pennsylvania 15282-1530, USA*
[3]*Laboratoire de Physique Théorique de la Matière Condensée, Université Pierre et Marie Curie, 4, place Jussieu, 75252 Paris Cedex 05, France*
(Received 4 October 2006; published 24 May 2007)

The kinetics of a granular planar rotator with a fixed center undergoing inelastic collisions with bath particles is analyzed both numerically and analytically by means of the Boltzmann equation. The angular velocity distribution evolves from quasi-Gaussian in the Brownian limit to an algebraic decay in the limit of an infinitely light particle. In addition, we compare this model to that of a planar rotator with a free center and discuss the prospects for experimental confirmation of these results.

DOI: 10.1103/PhysRevE.75.051307 PACS number(s): 45.70.−n, 05.20.Dd

I. INTRODUCTION

When macroscopic particles undergo inelastic collisions, the total kinetic energy decreases with time. If an external source of energy, such as a vibrating bottom wall, is present, the system may reach a stationary state. Despite similarities with equilibrium systems, however, equilibrium statistical mechanical concepts cannot be applied [1–3]. For instance, there is no equipartition between different species in polydisperse systems [4–9], and velocity distributions are, in general, non-Gaussian [10–13].

In dilute systems, most collisions involve only two particles, and consequently a theoretical description of the dynamics can be developed starting from the Boltzmann or Enskog equation [2,14]. This approach has been used to study tracer (or intruder) systems in which a single granular particle is immersed in a bath of thermalized particles.

When a spherical tracer particle undergoes inelastic collisions with the bath particles and when the collisions between bath particles are elastic, its granular temperature is lower than the bath temperature [6]. (When the collisions between bath particles are sufficiently inelastic, as compared with the tracer-bath collisions, and if the tracer particle is sufficiently massive, the tracer temperature can exceed that of the bath [15].) The velocity distribution function is, however, a pure Gaussian when the bath of particles is a Gaussian, whatever the coefficient of restitution [6,16,17]. Deviations from the Gaussian occur in a mixture composed of granular particles of finite density immersed in a thermostat, providing the energy via elastic collisions when this energy is redistributed within the granular component through inelastic encounters [9,18,19].

Few studies have addressed the effect of particle shape on the properties of granular gases. In three dimensions, Huthmann *et al.* [7] showed that the rotational and translational temperatures are different in the free cooling state of inelastic hard needles. Anisotropic tracers (needle and spherocylinder) in a thermalized bath also display nonequipartition between different degrees of freedom [20,21]. Unlike the case of a spherical tracer, here the angular velocity distribution function is not necessarily Gaussian when the bath particle distribution is Gaussian. Numerical studies showed no significant deviation from this distribution (which justified the use of a Gaussian ansatz in constructing an approximate theory). In a subsequent study [22], however, a power law was observed in the decay of the angular velocity of a needle with a fixed center of mass with sufficiently small moment of inertia.

In this paper we use a linear Boltzmann equation to examine the properties of the model over the entire parameter space of mass ratio and coefficient of restitution. We show that, when the tracer is much heavier than a bath particle, the angular velocity distribution function is quasi-Gaussian (the Brownian limit), whereas it exhibits an algebraic decay in the opposite limit of an infinitely light granular particle [22]. For all intermediate cases, there is no simple scaling regime, and deviations from Gaussian behavior are captured by analyzing the kurtosis of the distribution function. Even in the absence of the power law decay of the angular velocity distribution, there may be significant deviations from Gaussian behavior.

The paper is organized as follows. The model, its mechanical properties, and the Boltzmann equation are presented in Sec. II. The asymptotic solution of the Boltzmann equation in the Brownian limit is presented in Sec. III. In Sec. IV, analytical results are derived for the zero-mass limit and for different coefficients of restitution, and intermediate cases are considered in Sec. V. In Sec. VI we compare the fixed rotator with one whose center is free, both within the Gaussian approximation. Finally, the conclusion discusses possible experimental tests of our theoretical results.

II. THE PLANAR ROTATOR

A. Definition and mechanical properties

The model consists of a two-dimensional, infinitely thin needle of mass M, length L, and moment of inertia $I=ML^2/12$, immersed in a bath of point particles, each of mass m. The needle has a fixed center of mass, but can rotate freely around its center. It undergoes instantaneous and inelastic collisions with the surrounding bath particles. The motion of the planar rotator can be described by the angle between a unit vector $\mathbf{u}$ collinear with the axis of the needle and the x axis.

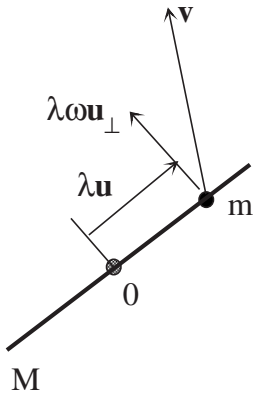

FIG. 1. Illustration of a collision between the planar rotator and a bath particle: $\mathbf{u}$ and $\mathbf{u}_\perp$ are unit vectors parallel and perpendicular to the axis of the rotator. The element of the needle at $\lambda\mathbf{u}$ moves with linear velocity $\lambda\omega\mathbf{u}_\perp$.

The rate of change of the orientation $\dot{\mathbf{u}}=\omega\mathbf{u}_\perp$ is equal to the angular velocity $\omega\in]-\infty,+\infty[$ times a unit vector $\mathbf{u}_\perp$ perpendicular to $\mathbf{u}$.

The angular velocity of the rotator changes at each binary collision with a bath particle. The position of the point of impact along the needle axis is denoted by $\lambda\mathbf{u}$. Obviously, a condition for collision is $|\lambda|<L/2$ (see Fig. 1). The relative velocity $\mathbf{V}$ at the point of impact is given by

$$\mathbf{V}=\mathbf{v}-\lambda\dot{\mathbf{u}}=\mathbf{v}-\lambda\omega\mathbf{u}_\perp, \tag{1}$$

where $\mathbf{v}$ denotes the velocity of the bath particle.

Due to the dissipative nature of the collision, the relative velocity changes according to the collision law

$$V_\perp^*=-\alpha V_\perp, \tag{2}$$

$$V_\parallel^*=V_\parallel, \tag{3}$$

where $0\leqslant\alpha\leqslant 1$ is the normal restitution coefficient, the indices $\perp$ and $\parallel$ indicate the perpendicular and parallel components of any vector relative to the needle axis, respectively, and postcollisional quantities are denoted with an asterisk. When $\alpha=1$, one recovers an elastic collision rule. For the sake of simplicity, the tangential component of the velocity is unchanged during the collision.

Since each collision conserves the total angular momentum we have that

$$I\omega^*+\lambda m v_\perp^*=I\omega+\lambda m v_\perp. \tag{4}$$

By combining Eqs. (1)–(4), the postcollisional bath particle velocity is given by

$$v_\perp^*=v_\perp-\frac{I(1+\alpha)V_\perp}{I+m\lambda^2}, \tag{5}$$

whereas the corresponding postcollisional angular velocity is

$$\omega^*=\omega+\frac{(1+\alpha)V_\perp m\lambda}{I+m\lambda^2}. \tag{6}$$

The inverse transformation (giving the precollisional quantities, denoted by a double asterisk) is obtained by substituting α by α^{-1} and the quantities with asterisks by quantities with double asterisks.

B. Homogeneous Boltzmann equation

At low density, one assumes that the needle influences weakly the local density of the bath and, consequently, that the system remains homogeneous. After a transient time (not considered here), the kinetics of the needle becomes stationary and can be described by the stationary Boltzmann equation. This expresses the invariance of the rotator angular velocity distribution function $F(\omega)$, resulting from a balance between collisional gain and loss terms:

$$\int_{-L/2}^{L/2}d\lambda\int d\mathbf{v}|v_\perp-\lambda\omega|\left(\frac{F(\omega^{**})\Phi_B(\mathbf{v}^{**})}{\alpha^2}-F(\omega)\Phi_B(\mathbf{v})\right),$$

$$=0 \tag{7}$$

where the precollisional velocities $\mathbf{v}^{**}$ and ω^{**} are given by the right-hand sides of Eqs. (5) and (6), respectively, with α replaced by α^{-1}. $\Phi_B(\mathbf{v})$ is the time-independent bath velocity distribution.

The integration over the parallel velocity component $v_\parallel$ in Eq. (7) can be readily carried out since F does not depend on this variable. This allows us to rewrite Eq. (7) as

$$\int_{-L/2}^{L/2}d\lambda\int dv_\perp|v_\perp|\left[F\left(w+v_\perp\frac{(1+\alpha)m\lambda}{I+m\lambda^2}\right)\right.$$
$$\left.\times\phi_B\left(\lambda\omega+v_\perp\frac{(\alpha m\lambda^2-I)}{I+m\lambda^2}\right)-F(\omega)\phi_B(v_\perp+\lambda\omega)\right]=0, \tag{8}$$

with $\phi_B(v)=\int dv_\parallel\Phi_B(|\mathbf{v}|)$.

III. BROWNIAN LIMIT

An exact solution of Eq. (8) cannot be obtained in general. When the mass of the planar rotator is much larger than the mass of the bath particle, however, one expects that the deviation from Maxwellian behavior is weak. It turns out (see Appendix A) that exploring the regime corresponding to Brownian motion is equivalent to the analysis of the small λ expansion of the collision term(8). We thus perform a perturbative expansion of the integrand of Eq. (8) in terms of λ. We denote

$$G(v_\perp,\omega,\lambda)=\left[F\left(w+v_\perp\frac{(1+\alpha)m\lambda}{I+m\lambda^2}\right)\right.$$
$$\times\phi_B\left(\lambda\omega+v_\perp\frac{(\alpha m\lambda^2-I)}{I+m\lambda^2}\right)$$
$$\left.-F(\omega)\phi_B(v_\perp+\lambda\omega)\right] \tag{9}$$

with the property that $G(v_\perp,\omega,0)=0$. To go further, we assume in the rest of this section that the bath distribution $\phi_B(v)$ is Maxwellian:

$$\phi_B(v) = \phi_M(v) = \sqrt{\frac{m}{2\pi T}} \exp(-mv^2/2T). \tag{10}$$

The first derivative of $G(v_\perp, \omega, \lambda)$ with respect to λ at $\lambda=0$ gives the differential equation

$$(1+\alpha)\frac{dF(\omega)}{d\omega} + 2F(\omega)\frac{\omega I}{T} = 0, \tag{11}$$

whose solution is

$$F(\omega) \propto \exp\left(-\frac{I\omega^2}{(1+\alpha)T}\right). \tag{12}$$

By taking the second derivative, one obtains the differential equation

$$(1+\alpha)\frac{d^2F(\omega)}{d\omega^2} + \frac{2I}{T}\omega\frac{dF(\omega)}{d\omega} + \frac{2I}{T}F(\omega) = 0, \tag{13}$$

whose solution is also given by Eq. (12).

The third-order expansion gives a polynomial in $v_\perp$,

$$\frac{m^3 v_\perp^3}{I^3} H_3(F(\omega)) - \frac{3m^2 v_\perp}{I^2} H_1(F(\omega)) = 0 \tag{14}$$

where

$$H_3(F(\omega)) = (1+\alpha)^3\frac{d^3F(\omega)}{d\omega^3} + 3(1+\alpha)^2\frac{I\omega}{T}\frac{d^2F(\omega)}{d\omega^2} + 3\frac{I}{T}\left((1+\alpha)\frac{I\omega^2}{T} + 2\right)\frac{dF(\omega)}{d\omega} + \frac{2I^2\omega}{T^2}\left(3(1+\alpha) + \frac{I\omega^2}{T}\right)F(\omega) \tag{15}$$

and

$$H_1(F(\omega)) = (1+\alpha)\left(2 + \frac{I\omega^2}{T}\right)\frac{dF(\omega)}{d\omega} + \frac{I\omega}{T}\left((1+\alpha) + 2\frac{I\omega^2}{T}\right)F(\omega). \tag{16}$$

The solution of $H_3=0$ is given by Eq. (12) again, but the solution of $H_1=0$ is

$$F(\omega) \sim \left(2 + \frac{I\omega^2}{T}\right)^{(1-\alpha)/(1+\alpha)} \exp\left(\frac{-I\omega^2}{(1+\alpha)T}\right). \tag{17}$$

Although Eq. (17) is different from Eq. (12), it is interesting to note that this solution is the same Maxwellian times a slowly decreasing function [if $\alpha=1$, Eq. (17) is identical to Eq. (12)]. The fourth derivative of $G(v_\perp, \omega, \lambda)$ has been calculated with the software MAPLE, and the differential equation associated with the $v_\perp^3$ term has a Maxwellian solution, but the solution of the differential equations associated with the $v_\perp$ term is given by the Maxwellian solution multiplied by a slowly varying function. Therefore, we conjecture that the complete solution is given by Eq. (12) times a subdominant term.

In order to check this assumption, we have solved numerically the Boltzmann equation. Since Eq. (8) is linear and the distribution $F(\omega)$ is a one-variable function, we have used an iterative method that is very efficient and provides a much more accurate solution [18] than a Direct Simulation Monte Carlo (DSMC) method [23,24].

The procedure consists of iterating the following equation:

$$F^{(n+1)}(\omega) = C(\omega)\int d\lambda \int dv |v| F^{(n)}\left(w + v\frac{(1+\alpha)m\lambda}{I+m\lambda^2}\right) \times \phi_B\left(\lambda\omega + v\frac{(\alpha m\lambda^2 - I)}{I+m\lambda^2}\right), \tag{18}$$

where

$$C(\omega) = \left(\int d\lambda \int dv |v - \lambda\omega| \phi_B(v)\right)^{-1}. \tag{19}$$

$C(\omega)$ is an explicit function when the bath particle distribution $\phi_B(v)$ is Maxwellian. The velocity distribution is sampled on a one-dimensional grid with 1000 points. The integrations over λ and ω are performed with Simpson's rule with 100 and 1500 points, respectively. For off-grid velocities, a linear interpolation is performed. The initial distribution is taken as the Maxwellian Eq. (12). Except when the mass of the planar rotator is extremely small, the method converges rapidly.

Figure 2(a) displays the (dimensionless) angular velocity distribution $F(\omega/\omega_0)$ (where $\omega_0=\sqrt{2T/I}$) for a mass ratio $M/m=10$ for different values of the coefficient of restitution α. The deviations from the Maxwellian distribution, shown in Fig. 2(b), increase with decreasing coefficient of restitution, but compared to the function $F(\omega)$ they vary weakly with the angular velocity. The iterative method allows us to obtain the tails of the distribution function with a higher precision than is possible obtained with a method (convergence occurs after few iterations when the mass ratio M/m is large and 50 iterations when the mass is 0.01). Figure 3 shows the angular velocity distributions for a mass ratio equal to 1. The deviations from the Gaussian behavior are more pronounced than those for a mass ratio of 10, but they are still negligible compared to the leading Gaussian term.

IV. ZERO-MASS LIMIT

When both the mass of the needle and the coefficient of restitution are equal to zero, the Boltzmann equation, Eq. (8), can be solved exactly [22]. Let us review the special characteristics of this limiting case. First, because the tracer particle has zero mass, the velocity of the bath particles never changes as the result of a collision. In addition, the angular velocity of the needle has no memory of its precollisional value. This quantity is reset after each collision, acquiring instantaneously the value $v_\perp/\lambda$. By introducing the variable $v_\perp=(\lambda\omega)y$, Eq. (8) can be written as

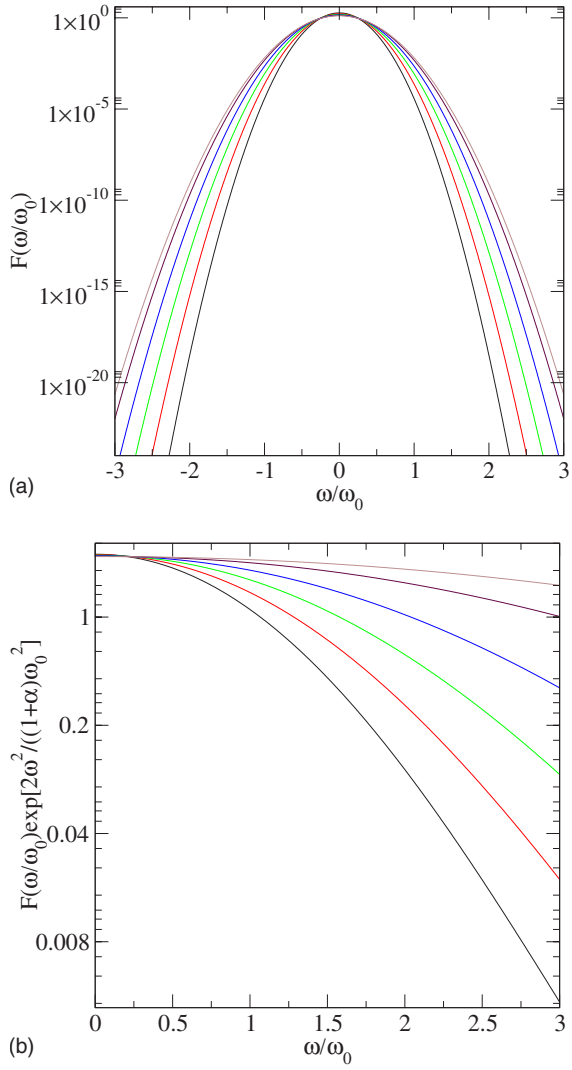

FIG. 2. (Color online) (a) Log_{10}-linear plot $F(\omega/\omega_0)$ for $M/m=10$ and with different values of the coefficient of restitution $\alpha=0,0.2,0.4,0.6,0.8,0.9$ (from top to bottom, center). (b) Log-linear plot $F(\omega/\omega_0)\exp[2(\omega^2/((1+\alpha)\omega_0^2)]$ for $M/m=10$.

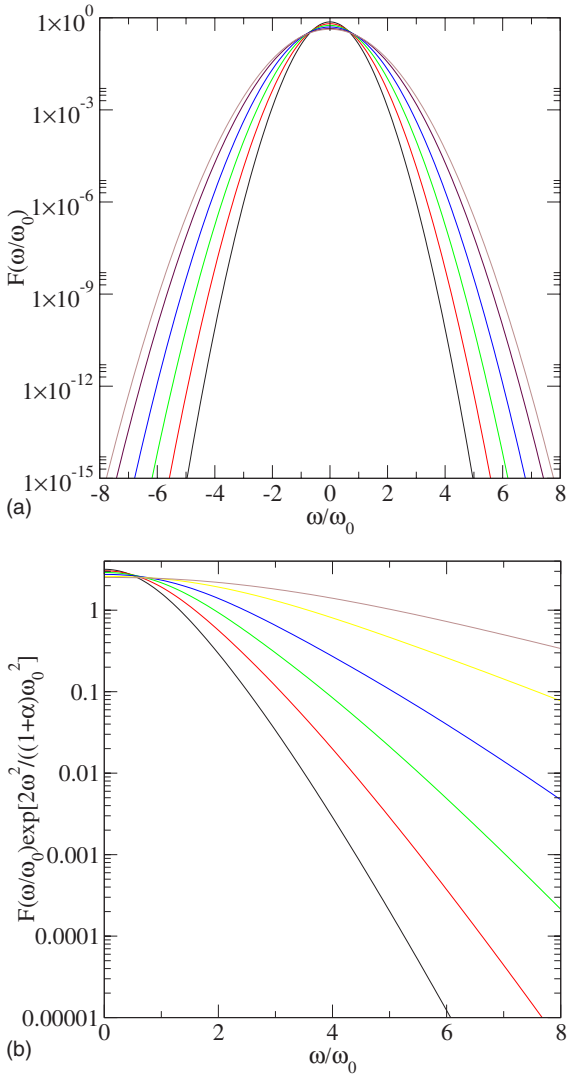

FIG. 3. (Color online) Same as Fig. 2 for $M/m=1$.

$$\int_{-L/2}^{L/2} d\lambda\, \lambda^2 \int dy|y| F\left(w\left(1+y\frac{(1+\alpha)m\lambda^2}{I+m\lambda^2}\right)\right) \times \phi_B\left(\lambda\omega\left(1+y\frac{(\alpha m\lambda^2 - I)}{I+m\lambda^2}\right)\right) = F(\omega)\int_{-L/2}^{L/2} d\lambda\, \lambda^2 \int dy|y-1|\phi_B(\lambda\omega y). \tag{20}$$

When $I=0$ and $\alpha=0$, this simplifies to

$$\int_{-L/2}^{L/2} d\lambda\, \lambda^2 \int dy|y| F(w(1+y))\phi_B(\lambda\omega) = F(\omega)\int_{-L/2}^{L/2} d\lambda\, \lambda^2 \int dy|y+1|\phi_B(\lambda\omega y). \tag{21}$$

The exact solution $F(\omega)$ of Eq. (21) is obtained by integrating the bath distribution $\phi_B(\lambda\omega)$ weighted by the position λ of the point of impact:

$$F(\omega) = \int_{-L/2}^{L/2} d\lambda \left(\frac{2\lambda}{L}\right)^2 \phi_B(\lambda\omega). \tag{22}$$

Note that this solution is independent of specific assumptions about the distribution of the bath particles. If we make the weak assumption that the second moment of the distribution $\phi_B(v)$ is finite, i.e., that the bath is characterized by a finite granular temperature, it can be shown that $F(\omega)$ decays algebraically as ω^{-3}. The long tail of $F(\omega)$ arises from collisions near the center of the rotator that result in large angular velocities. It is worth noting that solutions of the Boltzmann equation with power-law decay exist for isotropic particles, but not with a thermalized bath of particles [25,26].

While the granular temperature of the bath particles is finite, that of the tracer is not well defined, since its zero mass implies an infinite mean squared angular velocity. This difficulty is removed when the granular particle has a small but finite mass (see below).

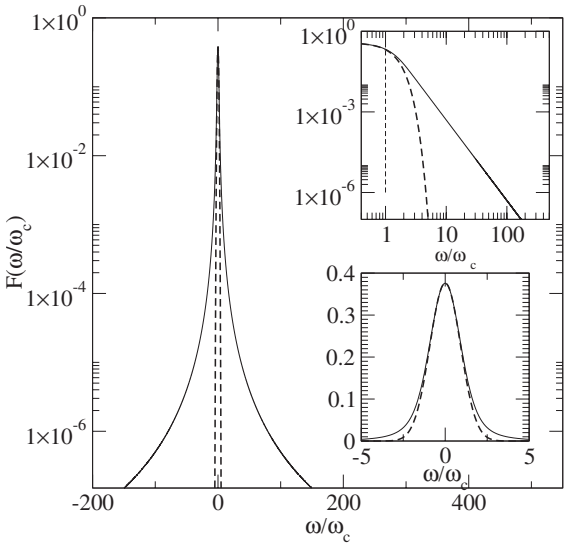

FIG. 4. Log_{10}-linear plot $F(\omega/\omega_c)$ of the "zero-mass" needle. The dashed curve corresponds to the Gaussian approximation obtained for $\omega<\omega_c$. The upper inset displays the log-log plot showing the power-law decay for sufficiently large ω values (the vertical dashed line corresponds to $\omega=\omega_c$), whereas the lower inset corresponds to a regular plot.

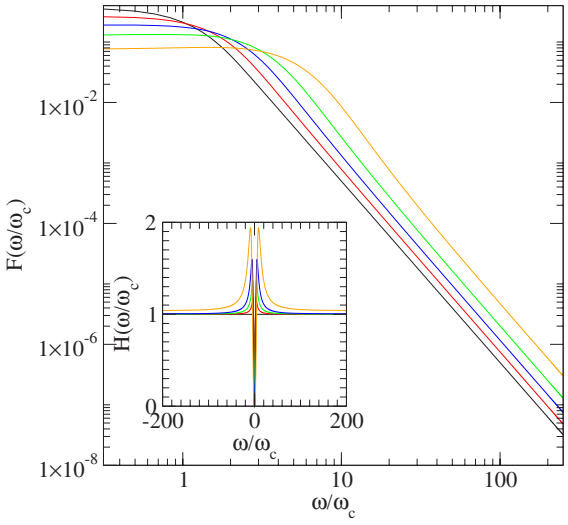

FIG. 5. (Color online) Log-log plot of $F(\omega/\omega_c)$ of the zero-mass needle with different values of the coefficient of restitution $\alpha=0,0.2,0.4,0.4,0.8$ from top to bottom. The inset shows the ω dependence of the rescaled function $H(\omega/\omega_c)=F(\omega/\omega_c)[(1-\alpha)/2(1+\alpha)]\omega^3/\omega_c^3$.

An explicit expression of the angular velocity distribution function $F(\omega)$ can be obtained when the bath particles have a Maxwellian velocity distribution $\phi_B(v)=\sqrt{m/2\pi T}\exp(-mv^2/2T)$. In this case

$$F(\omega) = -\sqrt{\frac{1}{\pi}}\frac{\omega_c}{\omega^2}\exp\left(-\frac{\omega^2}{\omega_c^2}\right)+\frac{\omega_c^2}{2\omega^3}\,\mathrm{erf}\left(\frac{\omega}{\omega_c}\right), \quad (23)$$

where $\omega_c=\sqrt{8T/(mL^2)}$ is the crossover frequency between two regimes. For $\omega>\omega_c$, $F(\omega)$ has a power-law behavior and for $\omega<\omega_c$, $F(\omega)\sim\exp[-3\omega^2/(5\omega_c^2)]$ is Gaussian (see Fig. 4). It is important to note that, when the power-law regime begins, the amplitude of $F(\omega)$ has only decreased by an order of magnitude compared to the maximum $F(0)$.

An obvious question is whether the behavior just described persists when either α or M/m is different from zero. Is the power-law regime sustained in these cases?

We first consider the case where the mass ratio is maintained at zero, but the coefficient of restitution is allowed to take all values between 0 and 1. For $\alpha=1$ (elastic collisions), the solution of the Boltzmann equation is the expected Maxwell distribution:

$$F(\omega) = \sqrt{\frac{I}{2\pi T}}\exp\left(-\frac{I\omega^2}{2T}\right), \quad (24)$$

but the limit $I\to 0$ does not yield a probability distribution.

For $0<\alpha<1$ and $I=0$, we were unable to obtain an analytical solution and we investigated the behavior numerically with the method described above. Figure 5 shows the logarithm of the distribution function versus the angular velocity. As in the case $\alpha=0$, two distinct regimes characterize $F(\omega)$: a scaling regime for $\omega>\omega_c(\alpha)$, where $\omega_c(\alpha)$ is a cutoff that increases with α, and a Gaussian behavior at low frequencies.

Figure 5 shows that, in the power-law regime, while the amplitude of $F(\omega)$ decreases when α increases, the exponent of the power law is independent of α. It is possible to obtain this result analytically by means of an asymptotic analysis of the Boltzmann equation, Eq. (21). Details of the calculation are given in Appendix B. The final result, for $M=0$ and $0<\alpha<1$, is

$$F(\omega) \sim \frac{(1+\alpha)\omega_c^2}{2(1-\alpha)\omega^3}. \quad (25)$$

Unlike the case where $\alpha=0$, here the rotator has a memory of its previous angular velocity after a collision with a bath particle, $\omega^*=\alpha\omega+(1+\alpha)v_\perp/\lambda$. This memory effect can be very small when a bath particle collides near the center of the rotator (small λ), which explains why, for large angular velocities, the distribution function behaves similarly to the case $\alpha=0$.

The inset of Fig. 5 displays $H(\omega)=F(\omega)[mL^2(1-\alpha)/4T(1+\alpha)]\omega^3$ versus ω, showing that the asymptotic behavior is rapidly reached and that the numerical results agree accurately with Eq. (25).

V. INTERMEDIATE CASES

We have considered in the preceding sections the two limiting cases of a large mass of the planar rotator (Brownian limit), where the angular velocity distribution function displays a Gaussian-like behavior, and the zero-mass case where, surprisingly, a solution of the Boltzmann equation exists with a power-law decay of the distribution function. In this section, we investigate the intermediate case that corresponds to most physical situations.

We consider a planar rotator with a small but finite mass $0<M\ll m$. In Eq. (8), since the integrand is an even function, integration can be restricted to positive values of λ. Moreover, the integral can be divided into two parts:

$$\int_0^{L/2} d\lambda = \int_0^{\epsilon} d\lambda + \int_{\epsilon}^{L/2} d\lambda, \tag{26}$$

where $\epsilon \gg \sqrt{I/m}$ (but ϵ being always small compared with $L/2$). For small angular velocities, the contribution of the first integral vanishes, and by performing a first-order expansion of the arguments of the integrand, one obtains

$$\int_{\epsilon}^{L/2} d\lambda\, F(\omega[1+y(1+\alpha)])\phi_B(\lambda(1+\alpha y)), \tag{27}$$

which leads to the Boltzmann equation of the massless particle when $\epsilon \to 0$.

Assigning a finite needle mass restores a finite granular temperature. For small mass M, the angular distribution function $F(\omega)$ behaves like the massless solution for $\omega<\omega_c^{(2)}$, i.e., a Gaussian for $\omega<\omega_c$ followed by a power law. For larger values of ω another Gaussian begins. The granular temperature T_n is given by the product of the moment of inertia times ω^2:

$$T_n = \int d\omega\, F(\omega) I\omega^2. \tag{28}$$

The integral can be divided into three contributions: the low-frequency range $[0,\omega_c]$, the intermediate power-law regime $[\omega_c,\omega_c^{(2)}]$, and the quasi-Gaussian region for $\omega>\omega_c^{(2)}$. Neglecting the α dependence, the upper cutoff $\omega_c^{(2)} \sim \omega_0$. Whereas the first and third contributions of the above integral remain finite when I decreases, the second contribution increases. Therefore, the granular temperature is dominated by the intermediate regime and is given by

$$T_n \sim 2\int_{\omega_c}^{\omega_0} \frac{d\omega}{\omega} I\omega_c^2 \sim I\omega_c^2 \ln\left(\frac{\omega_0}{\omega_c}\right) \sim T\frac{4I}{mL^2}\ln\left(\frac{mL^2}{4I}\right), \tag{29}$$

which means that the granular temperature of a planar rotator goes to zero as its mass decreases (even if the quadratic average of the angular velocity diverges logarithmically).

Figure 6 shows the distribution function for three small mass ratios $M/m=0.005,0.01,0.1$ with $\alpha=0$. As expected, the low-frequency distribution is well approximated by the massless distribution function. The inset shows that the range of the power-law decay decreases as the mass of the planar rotator increases. For large angular velocities, the distribution function resumes the Gaussian behavior, $F(w)\sim\exp\{-I\omega^2/[(1+\alpha)T]\}$, irrespective of the needle-to-bath particle mass ratio.

In summary, the velocity distribution "remembers" the massless solution up to the second crossover angular velocity $\omega_c^{(2)} \sim \omega_0$. If the mass of the planar rotator is sufficiently small, one observes three successive regimes: first, a Gaussian decay, second a power law, and finally, a Gaussian-like decay (subdominant terms are present).

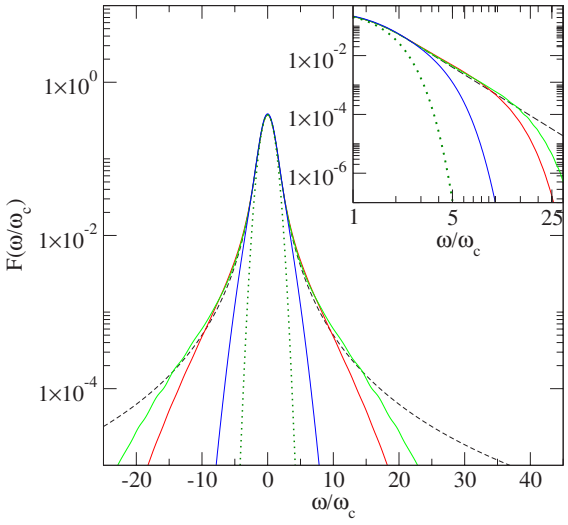

FIG. 6. (Color online) Log_{10}-linear plot of $F(\omega/\omega_c)$ for a needle with mass $M/m=0.005,0.01,0.1$. The width of the distributions decreases with the ratio M/m (dashed curve corresponds to $M=0.0$ and dotted curve to the Gaussian approximation). The inset shows the crossover between the power law and the Gaussian-like asymptotic.

When the masses of the planar rotator and a bath particle are comparable, the two crossover angular velocities merge and the power-law regime disappears. However, $F(\omega)$ may still deviate significantly from a Gaussian. In order to show this we introduce the quantity

$$\eta = \frac{\langle\omega^4\rangle}{3\langle\omega^2\rangle^2} - 1, \tag{30}$$

which is zero for a Gaussian distribution. Figure 7 displays η as a function of the coefficient of restitution α for different masses $M/m=0.1,1,2,10$.

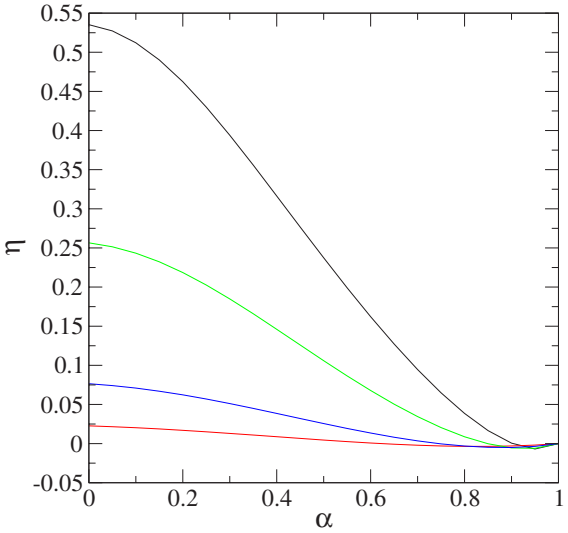

FIG. 7. (Color online) Deviations of the angular velocity distribution function from a Gaussian for $M/m=0.1,1,2,10$, top to bottom.

VI. MODELS WITH FREE OR FIXED CENTER

The model of granular planar rotator with a free center in a thermalized bath has been previously investigated by Viot and Talbot [20]. In this model, the tracer particle has, in addition to the rotational one, two translational degrees of freedom.

By using an approximate theory, as well as numerical simulations of the Boltzmann equation, it was shown that the translational and rotational granular temperatures are both smaller than the bath temperature, and also different from each other. In addition, the translational and rotational degrees of freedom are correlated [27].

In this section, we compare the rotational granular temperatures for the two models, all parameters being the same (mass ratio, coefficient of restitution, and bath temperature).

In order to obtain an analytical expression for the rotational temperature, we use a method originally proposed by Zippelius and colleagues that consists of calculating the second moment of the angular velocity of the Boltzmann equation [7,20,28]. In a stationary state, this quantity is constant, and by using a Gaussian ansatz for $F(\omega)$,

$$F(\omega) \propto \exp\left(\frac{-I\boldsymbol{\omega}^2}{2\bar{T}}\right), \tag{31}$$

one obtains a closed equation for the granular temperature $\bar{T}$ as a function of microscopic quantities:

$$\int_0^1 dx \frac{\bar{T}}{T} x^2 \frac{\sqrt{1+\frac{\bar{T}}{T}kx^2}}{1+kx^2} = \frac{1+\alpha}{2}\int_0^1 dx \frac{x^2\left(1+\frac{\bar{T}}{T}kx^2\right)^{3/2}}{(1+kx^2)^2}, \tag{32}$$

where

$$k = \frac{mL^2}{4I}. \tag{33}$$

Details of the calculation are given in Appendix C. Equation (32) is an implicit equation for $\bar{T}$, but, for a given value of α and of the mass ratio, it can be solved with standard numerical methods.

Figure 8 shows the variation of the rotational temperature with the normal coefficient of restitution for a mass ratio of 1 for a fixed (solid curve) and free (dashed curve) planar rotator. The temperature is always higher when the center is fixed except in the case of elastic collisions, $\alpha=1$. The circles correspond to the "exact" temperatures obtained by computing the second moment of the distribution function $F(\omega)$, which shows that the above method provides accurate approximate results for estimating the granular temperatures.

We also consider the variation of the granular temperature with the mass ratio for a given value of the restitution coefficient: See Fig. 9. It is easy to verify that in the Brownian limit, i.e., when the mass of the rotator is much larger than the particle mass, the granular temperature approaches $(1+\alpha)/2$, which is independent of the mass ratio and, probably, the shape of particle. As the mass of the needle decreases, the difference between the rotational temperatures of the free and fixed planar rotator increases. For elastic systems, the rotational temperatures remain identical for the two different situations (free or fixed center of mass), but significant differences occur for a granular particle.

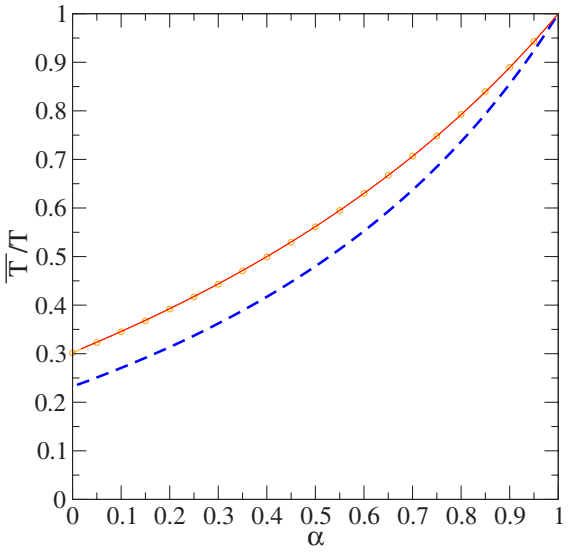

FIG. 8. (Color online) Effective granular temperature $\bar{T}$ as a function of the restitution of coefficient α for a fixed (full curve) and free rotator (dashed curve) in a bath of point particles. Circles correspond to the exact temperatures obtained by computing the second moment of the distribution function obtained by the numerical resolution. The mass ratio is $M/m=1$.

This phenomenon is more pronounced with varying mass ratio than with varying coefficient of restitution. Therefore, by monitoring the rotational motion of a granular needle in a bath of significantly heavier particles in two successive experiments (free and fixed center of mass), it should be possible to observe the absence of equipartition for a single particle.

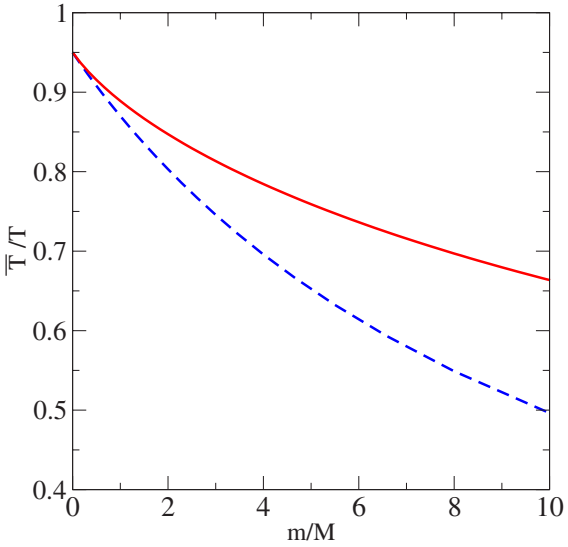

FIG. 9. (Color online) Effective granular temperature $\bar{T}$ as a function of the mass ratio M/m for a fixed (full curve) and free rotator (dashed curve) in a bath of point particles. The coefficient of restitution is $\alpha=0.9$.

VII. CONCLUSION

We have shown that the stationary angular velocity distribution of a planar rotator with a fixed center that collides inelastically with particles in a thermalized bath displays a variety of behavior as the mass of the rotator is changed. Starting from a quasi-Gaussian regime when the rotator is much heavier than the bath particle, $F(\omega)$ shows significant deviations from the Gaussian when the mass of the rotator is comparable to that of a bath particle. As the rotator mass decreases further, an intermediate power regime also appears.

We believe that these features are not specific to this simple model, but are generic for all granular systems containing nonspherical particles. Furthermore, we expect that the non-Gaussian character that is present in the idealized configuration of a thermalized bath will be amplified in the presence of a granular (nonthermal) bath. Several experiments on intensely vibrated granular systems using high-speed photography [5,29], image analysis, and particle tracking [4,30] have shown that many quantities, including granular temperature and velocity profiles, can be precisely measured. As recent experimental studies have demonstrated, some of the same techniques can also be applied to granular rods [31–35]. We believe that the significant difference between the granular temperatures of a free and fixed rotator that we have identified (Fig. 9) should be detectable using available experimental methods.

ACKNOWLEDGMENTS

J.P. acknowledges the Ministry of Science and Higher Education (Poland) for financial support (Research Project No. N20207631/0108). We thank Alexis Burdeau for helpful discussions.

APPENDIX A: DIMENSIONLESS BOLTZMANN EQUATION

In order to consider the Brownian motion regime, it is convenient to introduce dimensionless variables $\Omega = \sqrt{I/k_BT}\omega$ and $u_\perp = \sqrt{m/k_BT}v_\perp$.

In terms of these variables the integrand in the Boltzmann equation (8) takes the form

$$F\left(\Omega + u_\perp \frac{(1+\alpha)\epsilon}{1+\epsilon^2}\right)\phi_B\left(\Omega\epsilon + u_\perp \frac{\alpha\epsilon^2 - 1}{1+\epsilon^2}\right) - F(\Omega)\phi_B(u_\perp + \epsilon\Omega), \tag{A1}$$

where $\epsilon = \sqrt{m\lambda^2/I} = \sqrt{12m/M}\lambda/L$.

It is thus clear by inspection that the expansion of the dimensionless collision term (A1) in powers of ϵ is equivalent to the expansion of the collision term (8) in powers of λ. Notice that keeping the variable Ω fixed when exploring the region of $m \ll M$ corresponds to the Brownian motion asymptotics, as then the rotational energy $I\omega^2$ is maintained at a fixed ratio with the thermal energy k_BT.

APPENDIX B: ASYMPTOTIC BEHAVIOR OF THE ANGULAR VELOCITY DISTRIBUTION IN THE ZERO-MASS LIMIT

Performing the change of variable $u = \omega(y+1)$ in the left-hand side of Eq. (20) and $u = \omega y$ in the right-hand side, one obtains

$$\int_{-L/2}^{L/2} d\lambda\, \lambda^2 \int du |u-\omega| F((1+\alpha)u - \alpha\omega)$$

$$\phi_B(\lambda((1-\alpha)\omega + \alpha u)) = F(\omega)\int_{-L/2}^{L/2} d\lambda\, \lambda^2 \int du |u-\omega|\phi_B(\lambda u). \tag{B1}$$

When $|\omega| \to \infty$, one has

$$\int du |u-\omega|\phi_B(\lambda u) \sim \frac{|\omega|}{\lambda}, \tag{B2}$$

and therefore the right-hand side of Eq. (B1) becomes

$$F(\omega)\left(\frac{L}{2}\right)^2 |\omega|. \tag{B3}$$

Performing a similar analysis for the right-hand side of Eq. (B1), one gets the asymptotic relation of the Boltzmann equation (for the zero-mass limit),

$$F(\omega)\left(\frac{L}{2}\right)^2 = \int_{-L/2}^{L/2} d\lambda\, \lambda^2 \int du\, F((1+\alpha)u - \alpha\omega) \times \phi_B(\lambda((1-\alpha)\omega + \alpha u)). \tag{B4}$$

Let us introduce the Fourier transforms of the distribution functions $F(\omega)$ and $\phi_B(u)$ [with the convention $\hat{F}(k) = \int d\omega\, F(\omega)e^{-ikr}$]. The right-hand-side of Eq. (B4) can be expressed as

$$\int \frac{dk}{2\pi}\int \frac{dq}{2\pi}\int_{-L/2}^{L/2} d\lambda\, \lambda^2 \hat{F}(k)\hat{\phi}_B(q) \times \int du\, e^{ik[(1+\alpha)u - \alpha\omega]} e^{iq\lambda[(1-\alpha)\omega + \alpha u]}. \tag{B5}$$

By using the property $\int dx\, e^{iax} = 2\pi\delta(a)$, integration over v in Eq. (B5) can be carried out, and one obtains

$$\int \frac{dq}{2\pi}\int_{-L/2}^{L/2} d\lambda\, \lambda^2 \hat{F}\left(\frac{\lambda\alpha q}{1+\alpha}\right)\frac{\hat{\phi}_B(q)}{1+\alpha} e^{i\omega[\lambda q/(1+\alpha)]}. \tag{B6}$$

By taking the Fourier transform of Eq. (B4) and by using Eq. (B6), the asymptotic form of the Boltzmann equation becomes

$$\hat{F}(k)\left(\frac{L}{2}\right)^2 = \hat{F}(\alpha k)\int_{-L/2}^{L/2} d\lambda |\lambda| \hat{\phi}_B\left(\frac{1+\alpha}{\lambda} q\right). \tag{B7}$$

The integral of the right-hand side of Eq. (B7) can explicitly performed:

$$\int_{-L/2}^{L/2} d\lambda |\lambda| \hat{\phi}_B\left(\frac{1+\alpha}{\lambda} q\right) = \int_0^1 d\mu \exp\left(-2\frac{(1+\alpha)^2 k^2 T}{\mu m L^2}\right) = \exp\left(-2\frac{(1+\alpha)^2 k^2 T}{mL^2}\right) \times -2\frac{(1+\alpha)^2 k^2 T}{mL^2} E_i\left(1, 2\frac{(1+\alpha)^2 k^2 T}{mL^2}\right), \quad \text{(B8)}$$

where $E_i(1,x)$ is the exponential integral. For small values of k, Eq. (B8) behaves as

$$\int_{-L/2}^{L/2} d\lambda\, \lambda \hat{\phi}_B\left(\frac{1+\alpha}{\lambda} q\right) \simeq 1 + 4\frac{(1+\alpha)^2 T}{mL^2} k^2 \ln(|k|). \quad \text{(B9)}$$

Inserting Eq. (B9) in Eq. (B7) yields

$$\hat{F}(k)\left(\frac{L}{2}\right)^2 = \hat{F}(\alpha k)\left(1 + 4\frac{(1+\alpha)^2 T}{mL^2} k^2 \ln(|k|)\right). \quad \text{(B10)}$$

Iterating Eq. (B10) and by using that $\hat{F}(k)=1$, one obtains that

$$\hat{F}(k) = 1 + \frac{1+\alpha}{1-\alpha}\frac{4T}{mL^2} k^2 \ln(|k|). \quad \text{(B11)}$$

The inverse Fourier transform of Eq. (B11) leads to Eq. (25).

APPENDIX C: GRANULAR ROTATIONAL TEMPERATURE OF THE PLANAR ROTATOR WITH A GAUSSIAN APPROXIMATION

By taking the second moment of Eq. (7), one obtains the following equation:

$$\int_{-L/2}^{L/2} d\lambda \int v \int d\omega\, \theta(\omega\lambda - v)|v - \omega\lambda| F(\omega)\phi_B(v)\Delta\omega^2 = 0, \quad \text{(C1)}$$

where $\Delta\omega^2 = \omega^{*2} - \omega^2$. This equation means that for a stationary state the second moment of the distribution is time independent, or, in other words, that the loss of the rotational energy of the planar rotator induced by inelastic collisions is compensated on average by collisions with bath particles with higher velocities.

By using Eq. (6), the difference between the square angular velocities at a collision is given by

$$\Delta\omega^2 = -\lambda(1+\alpha)\frac{\mathbf{V}\cdot\mathbf{u}_\perp(\omega^* + \omega)}{I/m + \lambda^2} = -2\lambda(1+\alpha)\frac{\mathbf{V}\cdot\mathbf{u}_\perp\omega}{I/m+\lambda^2} + \lambda^2(1+\alpha)^2\frac{(\mathbf{V}\cdot\mathbf{u}_\perp)^2}{(I/m+\lambda^2)^2}. \quad \text{(C2)}$$

We introduce the dimensionless vectors

$$\mathbf{s} = (s_x, s_y) = \left(\sqrt{\frac{m}{2T}} v, \sqrt{\frac{I}{2\bar{T}}}\omega\right) \quad \text{(C3)}$$

and

$$\mathbf{G} = (G_x, G_y) = \left(\sqrt{\frac{2T}{m}}, \sqrt{\frac{2\bar{T}}{I}}\lambda\right) \quad \text{(C4)}$$

Therefore the scalar product $\mathbf{G}\cdot\mathbf{s}$ gives

$$\mathbf{G}\cdot\mathbf{s} = v - \omega\lambda. \quad \text{(C5)}$$

Equation (C1) can be expressed as

$$\int_{-L/2}^{L/2} d\lambda \int d\mathbf{s} \exp(-\mathbf{s}^2)\theta(-\mathbf{G}\cdot\mathbf{s})|\mathbf{G}\cdot\mathbf{s}| \times\left[-\frac{2\lambda(1+\alpha)\mathbf{G}\cdot\mathbf{s}}{I/m+\lambda^2}\sqrt{\frac{2\bar{T}}{I}} s_y + \frac{\lambda^2(1+\alpha)^2(\mathbf{G}\cdot\mathbf{s})^2}{(I/m+\lambda^2)^2}\right] = 0. \quad \text{(C6)}$$

Let us define a new coordinate system [28] where the y axis is parallel to $\mathbf{G}$: unit vectors are denoted $(\mathbf{e}_1, \mathbf{e}_2)$ whereas the unit vectors of the original system were $(\mathbf{e}_x, \mathbf{e}_y)$. It follows that $\mathbf{G} = |\mathbf{G}|\mathbf{e}_1$ and therefore one can write that

$$\mathbf{G}\mathbf{e}_1\mathbf{e}_y = |\mathbf{G}|\mathbf{e}_x = G_x. \quad \text{(C7)}$$

Inserting Eq. (C7) in Eq. (C6) allows for performing standard Gaussian integrals and finally one obtains Eq. (32)

[1] I. Goldhirsch, Annu. Rev. Fluid Mech. **35**, 267 (2003).
[2] N. V. Brilliantov and T. Pöschel, *Kinetic Theory of Granular Gases* (Oxford University Press, Oxford, 2004).
[3] A. Zippelius, Physica A **369**, 143 (2006).
[4] R. D. Wildman and D. J. Parker, Phys. Rev. Lett. **88**, 064301 (2002).
[5] K. Feitosa and N. Menon, Phys. Rev. Lett. **88**, 198301 (2002).
[6] P. A. Martin and J. Piasecki, Europhys. Lett. **46**, 613 (1999).
[7] M. Huthmann, T. Aspelmeier, and A. Zippelius, Phys. Rev. E **60**, 654 (1999).
[8] A. Barrat and E. Trizac, Granular Matter **4**, 57 (2002).
[9] V. Garzó and J. Dufty, Phys. Rev. E **60**, 5706 (1999).
[10] F. Rouyer and N. Menon, Phys. Rev. Lett. **85**, 3676 (2000).
[11] J. Atwell and J. S. Olafsen, Phys. Rev. E **71**, 062301 (2005).
[12] J. J. Brey, D. Cubero, and M. J. Ruiz-Montero, Phys. Rev. E **59**, 1256 (1999).
[13] T. P. C. van Noije and M. H. Ernst, Granular Matter **1**, 57 (1998).
[14] T. Pöschel and N. Brilliantov, *Granular Gas Dynamics* (Springer, Berlin, 2003).
[15] A. Santos and J. W. Dufty, e-print arXiv:cond-mat/0608604.
[16] A. Santos and J. W. Dufty, Phys. Rev. Lett. **97**, 058001 (2006).

[17] J. Piasecki, J. Talbot, and P. Viot, Physica A **373**, 313 (2006).
[18] T. Biben, P. A. Martin, and J. Piasecki, Physica A **310**, 308 (2002).
[19] A. Santos, Phys. Rev. E **67**, 051101 (2003).
[20] P. Viot and J. Talbot, Phys. Rev. E **69**, 051106 (2004).
[21] H. Gomart, J. Talbot, and P. Viot, Phys. Rev. E **71**, 051306 (2005).
[22] J. Piasecki and P. Viot, Europhys. Lett. **74**, 1 (2006).
[23] G. Bird, *Molecular Gas Dynamics and the Direct Simulation of Gas Flows* (Clarendon Press, Oxford, 1994).
[24] J. M. Montanero and A. Santos, Granular Matter **2**, 53 (2000).
[25] E. Ben-Naim and J. Machta, Phys. Rev. Lett. **94**, 138001 (2005).
[26] E. Ben-Naim, B. Machta, and J. Machta, Phys. Rev. E **72**, 021302 (2005).
[27] J. Talbot and P. Viot, J. Phys. A **39**, 10947 (2006).
[28] T. Aspelmeier, T. M. Huthmann, and A. Zippelius, *Granular Gases* (Springer, Berlin, 2001), p. 31.
[29] K. Feitosa and N. Menon, Phys. Rev. Lett. **92**, 164301 (2004).
[30] R. D. Wildman, J. M. Huntley, and D. J. Parker, Phys. Rev. Lett. **86**, 3304 (2001).
[31] D. L. Blair, T. Neicu, and A. Kudrolli, Phys. Rev. E **67**, 031303 (2003).
[32] D. Volfson, A. Kudrolli, and L. S. Tsimring, Phys. Rev. E **70**, 051312 (2004).
[33] J. Galanis, D. Harries, D. L. Sackett, W. Losert, and R. Nossal, Phys. Rev. Lett. **96**, 028002 (2006).
[34] G. Lumay and N. Vandewalle, Phys. Rev. E **70**, 051314 (2004).
[35] G. Lumay and N. Vandewalle, Phys. Rev. E **74**, 021301 (2006).